ROYAL SOCIETY OPEN SCIENCE

royalsocietypublishing.org/journal/rsos

Research

Cite this article: Sun S, Zhang C, Chen S, Zhao X, Wang Y, Xu S, Wu C. 2023 Integrated CO_2 capture and reverse water–gas shift reaction over CeO_2-CaO dual functional materials. *R. Soc. Open Sci.* **10**: 230067.
https://doi.org/10.1098/rsos.230067

Received: 20 January 2023
Accepted: 13 February 2023

Subject Category:
Chemistry

Subject Areas:
environmental chemistry/materials science/chemical engineering

Keywords:
integrated CO_2 capture and utilization, reverse water–gas shift reaction, dual functional materials, carbon capture, CaO

Authors for correspondence:
Shaojun Xu
e-mail: shaojun.xu@manchester.ac.uk
Chunfei Wu
e-mail: c.wu@qub.ac.uk

This article has been edited by the Royal Society of Chemistry, including the commissioning, peer review process and editorial aspects up to the point of acceptance.

ROYAL SOCIETY OF CHEMISTRY

THE ROYAL SOCIETY PUBLISHING

Integrated CO_2 capture and reverse water–gas shift reaction over CeO_2-CaO dual functional materials

Shuzhuang Sun[1], Chen Zhang[1], Sining Chen[2,3], Xiaotong Zhao[1], Yuanyuan Wang[1], Shaojun Xu[3,4,5] and Chunfei Wu[1]

[1]School of Chemistry and Chemical Engineering, Queen's University Belfast, Belfast BT7 1NN, UK
[2]Department of Chemistry, University College London, 20 Gordon Street, London WC1H 0AJ, UK
[3]UK Catalysis Hub, Research Complex at Harwell, Didcot OX11 0FA, UK
[4]Department of Chemical Engineering, University of Manchester, Manchester M13 9PL, UK
[5]Cardiff Catalysis Institute, School of Chemistry, Cardiff University, Cardiff CF10 3AT, UK

SS, 0000-0003-1573-8713; CZ, 0000-0003-4767-7732; SC, 0000-0003-4706-5699; XZ, 0000-0002-5356-6361; YW, 0000-0001-6111-4392; SX, 0000-0002-8026-8714; CW, 0000-0001-7961-1186

Achieving carbon neutrality is one of the most important tasks to meet the environmental challenges due to excessive CO_2 emissions. Integrated CO_2 capture and utilization (ICCU) represents an effective process for direct utilization of CO_2-contained exhaust gas (e.g. flue gas), in which converting the captured CO_2 into CO via reverse water–gas shift (RWGS) reaction is a promising route. The dual functional materials (DFMs), containing CO_2 adsorbents and catalysts, are widely applied to achieve ICCU. The conventional active metals (Ni, Fe, etc.)-based DFMs and non-transition metal DFMs (e.g. CaO) are restricted by low CO selectivity, catalytic efficiency or CO generation in the CO_2 capture step. To address the above obstructs in the application of DFMs, the metal oxides-based DFMs, MO_x-CaO (M = Al, Ce, Ti or Zr), are synthesized and evaluated. The CeO_2-CaO outperformed the other metal oxides-based DFMs and possessed significantly improved catalytic performance. It is found that 33% CeO_2-CaO DFM displayed approximately 49% CO_2 conversion and approximately 100% CO selectivity in integrated CO_2 capture and reverse water–gas shift reaction (ICCU-RWGS) at 650°C, while CaO-alone only achieved approximately 20% CO_2 conversion at the same condition. The surface basicity of CeO_2 is revealed to contribute to the improved catalytic performance by enhancing CO_2 chemisorption and activation in the hydrogenation step. Furthermore, CeO_2-CaO material possessed excellent cycle

stability in 20 cycles ICCU-RWGS, achieving a sustainable and high-efficient performance in CO_2 conversion and CO selectivity.

1. Introduction

Numerous countries have pledged to achieve carbon neutrality around the mid-twenty-first century to eliminate the severe greenhouse effect and accompanying environmental issues [1]. However, in the foreseeable future, it is still inevitable to use fossil fuels to meet the energy demands [2], which would emit a huge amount of CO_2. Carbon dioxide capture and utilization or storage (CCUS) processes are believed to be effective and essential solutions to meet the great challenges for carbon neutrality [3–6]. However, the high capital costs of CCUS processes [7], including CO_2 enrichments, transportation and heat management, obstruct the industrial deployments.

To directly use the diluted CO_2 in the exhaust gas, integrating CO_2 capture with utilization (ICCU) [8–10] into one process exhibits an impressive performance and attractive application potential [11]. Specifically, the ICCU process can be achieved by swinging the inlet gas between exhaust gas (e.g. flue gas) and reducing agent (e.g. H_2) isothermally over the dual functional materials (DFMs). The majority of researchers paid attention to converting captured CO_2 into CH_4 [8,12–16], which is mainly re-used as fuel with equivalent carbon emissions. Recently, researchers have achieved CO generation via ICCU by reverse water–gas shift reaction (ICCU-RWGS) [17–20]. The unconsumed H_2 mixed with CO (syn-gas) can be further introduced into the Fischer–Tropsch synthesis process to produce high-end chemicals (e.g. olefins), which possess a longer life cycle compared with fuels [21]. Various metal-functionalized CaO DFMs were demonstrated to realize ICCU-RWGS, such as Ni-CaO [18,19,22,23], $Fe_xCo_yMg_{10}CaO$ [17], FeCrCu/K/hydrotalcite [24] and Fe-CaO [19,25]. Although the introduction of metals (e.g. Ni, Fe or Co) contributes to the effective catalytic RWGS in ICCU, the CO selectivity and undesirable CO generation during CO_2 capture restrict the further deployment [19]. Specifically, the CO generation in the CO_2 capture process is attributed to the reaction between CO_2 and reduced metallic metal (e.g. Fe) [25]. In recent study, removing transition metals from DFMs shows reduced CO generation during CO_2 capture and improved CO selectivity during the conversion of adsorbed CO_2 [26,27]. However, the absence of active metals significantly reduced the hydrogenation efficiency of DFMs and further restricted the cycle efficiency of ICCU. In short, there is a trade-off between impurity (i.e. CO) generation in the CO_2 capture process and the catalytic efficiency and CO selectivity in the RWGS process. It is necessary to develop novel DFMs to avoid CO generation in the CO_2 capture process while achieving enhanced RWGS efficiency with excellent CO selectivity.

Metal oxides (such as CeO_2 and TiO_2) are believed to be catalytically active in many reaction processes [28], such as reforming processes, photocatalysis and water–gas shift reaction [29]. Those metal oxides so far are mainly applied in ICCU by acting as the catalyst support for the active metal species [18,30,31]. However, there is still a knowledge gap in understanding the catalytic roles and other promotion effects of the metal oxides in DFMs during the ICCU process. Herein, we investigated ICCU performance over the DFMs composing various metal oxides (CeO_2, TiO_2, ZrO_2 and Al_2O_3)-CaO DFMs, in which CeO_2 is identified as the active metal oxide, while other metal oxides are benchmarks. The DFMs were produced by physically mixing the metal oxides and CaO. As illustrated in figure 1, the DFMs firstly act as the adsorbents to reduce the CO_2 emissions via carbonation, subsequently, the carbonated DFMs are converted in the H_2 atmosphere with the formation of CO. The catalytic performances of various DFMs and cycle stability were real-time studied using an online gas analyser and discussed with characterizations, in order to reveal the effect of the non-active metal containing CeO_2-CaO DFM on promoting the ICCU-RWGS.

2. Experimental section

2.1. Preparation of MO_x-CaO (M = Al, Ce, Ti or Zr) dual functional materials

The CeO_2 was synthesized using a hydrothermal method as previously reported [15,16]. Specifically, 5.21 g $Ce(NO_3)_3{\cdot}6H_2O$ (Sigma-Aldrich, 99%) was dissolved in deionized water (30 ml) to prepare a Ce source solution, followed by the dissolution of 57.6 g NaOH (Sigma-Aldrich, 99%) in deionized water (210 ml) to prepare the precipitant. The Ce source was mixed with the precipitant dropwise for 30 min at room temperature to obtain a slurry. The slurry was transferred into a stainless-steel autoclave and

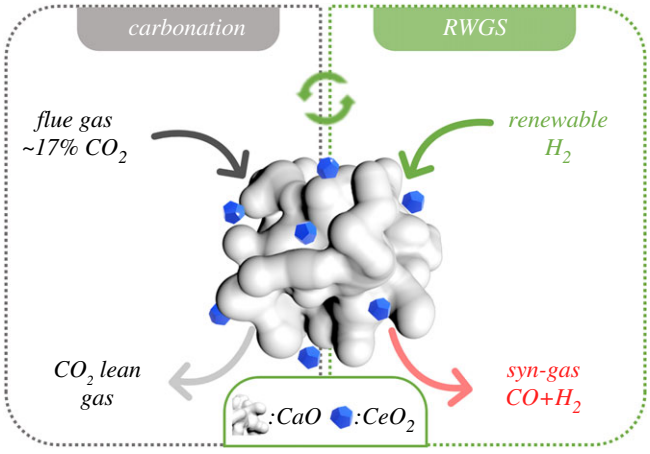

Figure 1. Schematic diagram of ICCU-RWGS.

kept at 100°C for 24 h. The precipitate was washed and separated by vacuum filtration using distilled water and ethanol to neutrality and dried at 120°C overnight, to produce a yellow powder, labelled as CeO_2. The ZrO_2 (Sigma-Aldrich, 99%), TiO_2 (Sigma-Aldrich, 99.5%), Al_2O_3 (Sigma-Aldrich, 99.5%) and CeO_2 were calcined at 800°C for 2 h with a heating rate of 5°C min^{-1} before mixing with CaO.

The CaO was derived by a sol–gel method as reported in previous literatures [19,25]. Briefly, 23.6 g $Ca(NO_3)_2{\cdot}4H_2O$ (Sigma-Aldrich, 99%) and 19.2 g citric acid monohydrate (Sigma-Aldrich, 99.5%) were dissolved into 72 ml distilled water, stirred at room temperature at 80°C and dried at 120°C overnight. The sample was ground and calcined at 850°C for 5 h at a heating rate of 5°C min^{-1} to obtain CaO.

The MO_x (M = Al, Ce, Ti or Zr) and CaO are physically mixed by grinding (mass ratio: MO_X : CaO = 1 : 2) to prepare the MO_x-CaO DFMs.

2.2. Characterizations

X-ray diffraction (XRD) patterns of MO_x (M = Al, Ce, Ti or Zr) were measured using a PANalytical Empyrean Series 2 diffractometer with a Cu Ka X-ray source. The CO_2 temperature-programmed desorption (CO_2-TPD) patterns of MO_x (M = Al, Ce, Ti or Zr) were measured by a Micromeritics Autochem II 2920 analyser equipped with a TCD detector. Briefly, the MO_x were *in situ* reduced at 550°C in H_2 for 1 h and then cooled down to 30°C under He. After adsorbing CO_2 in a 10% CO_2/He gas mixture at 30°C, the temperature was increased to 800°C in He at a heating rate of 10°C min^{-1}. Scanning electron microscopy coupled with an energy-dispersive X-ray spectrometer (SEM-EDX, FEI Quanta FEG) was used to characterize the morphology and element dispersion.

2.3. Integrated CO_2 capture and reverse water–gas shift reaction evaluation

The ICCU-RWGS performances of MO_x-CaO DFMs were evaluated on a tubular fixed-bed reactor (stainless-steel tube; 500.0 mm in length and 10.2 mm in inner diameter). The reactor was placed in the middle of the furnace (Elite TSH-2416CG), filled with 0.3 g DFMs catalyst with quartz wool on both end of the catalysts. The thermocouple was placed in the middle of DFMs to control the temperature. The flow rates of the inlet gases were controlled by mass flow meters (OMEGA FMA2300), and the outlet gas (CO_2, CO and CH_4) was monitored by an online gas analyser (Kane Autoplus 5).

The typical ICCU-RWGS reaction procedure includes mainly two steps, i.e. carbonation and hydrogenation. In this work, all the DFMs catalysts were pretreated in 100 ml min^{-1} 5% H_2/N_2 at 550°C for 1 h to clean the surface of the catalysts and then equilibrated to the defined evaluation temperature in the range of 600–750°C in 100 ml min^{-1} N_2. In the carbonation step, 100 ml min^{-1} 17% CO_2/N_2 (no added steam and O_2) was introduced for 1700 s to ideally simulate flue gas CO_2 capture. Subsequently, the hydrogenation step is to switch the gas to 5% H_2/N_2 at 100 ml min^{-1} to convert CO_2 and regenerate the adsorbent. The cycle evaluations were carried out with extra 5 min N_2 purge among each ICCU-RWGS procedure.

The real-time CO_2 conversion, CO generation rate and CO selectivity in RWGS were calculated as equations (2.1)–(2.3).

$$C_{CO2} = \frac{CO + CH_4}{CO + CH_4 + CO_2}\%, \tag{2.1}$$

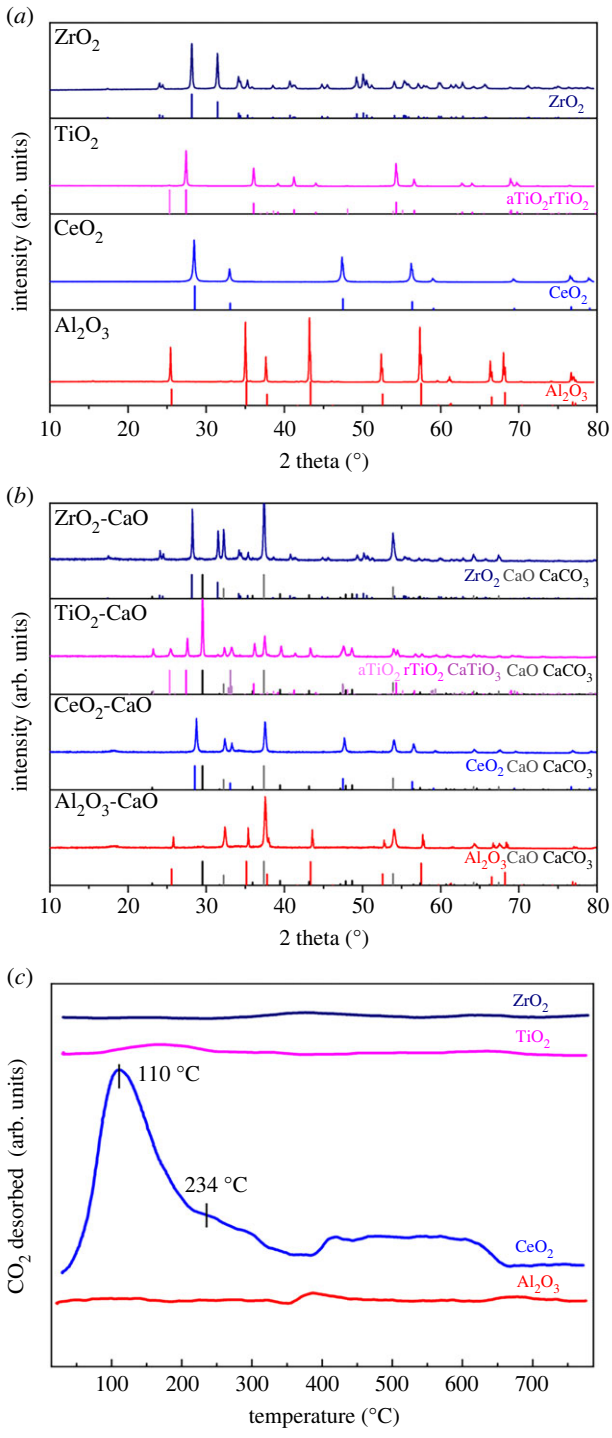

Figure 2. XRD patterns of (*a*) MO_x and (*b*) spent MO_x-CaO; (*c*) CO_2-TPD profiles of MO_x (M = Al, Ce, Ti or Zr).

$$Y_{CO} = \frac{CO(\%) \times 1.667 \text{ ml s}^{-1}}{0.0224 \text{ ml } \mu\text{mol}^{-1} \times 0.30 \text{ g}} \tag{2.2}$$

and

$$S_{CO} = \frac{CO}{CO + CH_4}\% , \tag{2.3}$$

where C_{CO2}, Y_{CO} and S_{CO} represent CO_2 conversion (%), CO generation rate (μmol g_{DFM} s^{-1}) and CO selectivity (%). The catalytic performance (CO_2 conversion, CO yield and CO selectivity) throughout the hydrogenation step was evaluated by the integration of real-time CO_2 conversion, CO generation rate and CO selectivity.

Table 1. Pore information of MO_x materials.

materials	BET surface area $m^2\ g^{-1}$	pore volume $cm^3\ g^{-1}$
ZrO_2	5.46	0.02
TiO_2	11.85	0.03
CeO_2	65.76	0.25
Al_2O_3	0.65	<0.01

3. Results and discussions

3.1. Characterizations of MO_x (M = Al, Ce, Ti or Zr)

The XRD patterns of the produced metal oxides (MO_x) are shown in figure 2*a*. The CeO_2 and the benchmarks Al_2O_3, TiO_2 and ZrO_2 all possess pure crystal phase after elevated temperature pretreatment and are consistent with PDF75-1864, PDF78-0694, PDF75-1753 (rutile, $rTiO_2$), PDF83-2243 (anatase, $aTiO_2$) and PDF86-1451, respectively. Al_2O_3, ZrO_2 and CeO_2 performed no interaction with CaO during ICCU evaluation, while the TiO_2 formed a small amount of $CaTiO_3$ with CaO (figure 2*b*). The CO_2-TPD profiles are shown in figure 2*c* to evaluate the basicity of MO_x. Notably, only CeO_2 possessed distinct CO_2 desorption peaks, while the other three benchmark MO_x exhibited negligible basic property. For the CO_2 desorption on CeO_2, two major CO_2 desorption peaks appear at 110 and 234°C, representing the weak and medium basic sites, respectively [32,33]. Furthermore, the CeO_2 material exhibits weak high-temperature CO_2 desorption signal (400–600°C), which might be attributed to the strong interaction of CO_2 and CeO_2 [33]. The basicity of the catalyst is believed to benefit the adsorption and catalytic activation of CO_2 in CO_2 reduction process. The porosity of MO_x is highly related to the diffusion of reactants and exposure of active sites. As summarized in table 1, the CeO_2 exhibited the most abundant pores, which might contribute to the CO_2 diffusion, chemisorption and then activation in ICCU.

3.2. Integrated CO_2 capture and reverse water–gas shift reaction performance over MO_x-CaO dual functional materials

The real-time catalytic performances of ICCU-RWGS using MO_x-CaO (M = Al, Ce, Ti or Zr) DFMs are presented in figure 3. The Al_2O_3 TiO_2 and ZrO_2 are widely recognized as inert materials in thermal catalytic processes, which are applied as the benchmark in this work. To strictly exclude the potential effects of inert metal oxides on ICCU-RWGS, 0.2 g CaO without any MO_x (M = Al, Ce, Ti or Zr) was also evaluated for comparison. In the previous work [19,26], 650°C was suggested as the optimal temperature for CaO in ICCU based on the carbonation-decarbonation kinetics. Herein, the ICCU-RWGS evaluations using physically mixed MO_x and CaO formed DFMs (MO_x-CaO) were firstly carried out at 650°C (figure 3).

As shown in figure 3*a*, the CaO in DFMs capture CO_2 via carbonation from a 100 ml min^{-1} 17% CO_2/N_2 gas mixture (simulating flue gas) for 1700 s. After that, the carbonated MO_x-CaO DFMs were reduced in a 5% H_2/N_2 at 100 ml min^{-1} for reverse water–gas shift reaction (RWGS), as shown in figure 3*a*. The real-time carbonated CO_2 conversion possessed a gradually increasing trend as a function of time in the hydrogenation step. In the initial stage, the CO_2 conversion was hindered by the fast CO_2 release rate ascribed to the rapid decomposition of surface carbonates [19], which decreases the H_2 partial pressure (i.e. concentration) around DFMs and hinders the CO_2 conversion with H_2. With the consumption of the surface carbonates, the subsurface carbonate species exhibit a slower CO_2 release rate, then the increased H_2 partial pressure over the surface of the DFMs enhanced CO_2 hydrogenation performance with increased CO_2 conversion as shown in figure 3*b*. The inhibition of CO_2 release on the enhancement of the catalytic performance can be further evidenced by the real-time CO generation rate (figure 3*b*). In the initial approximately 250 s hydrogenation, the CO generation rate was even lower than 0.5 μmol g_{DFM} s^{-1} on all tested DFMs. Notably, all the tested DFMs exhibited excellent CO selectivity (greater than 99%), which outperformed the commonly applied Ni-based DFMs [19].

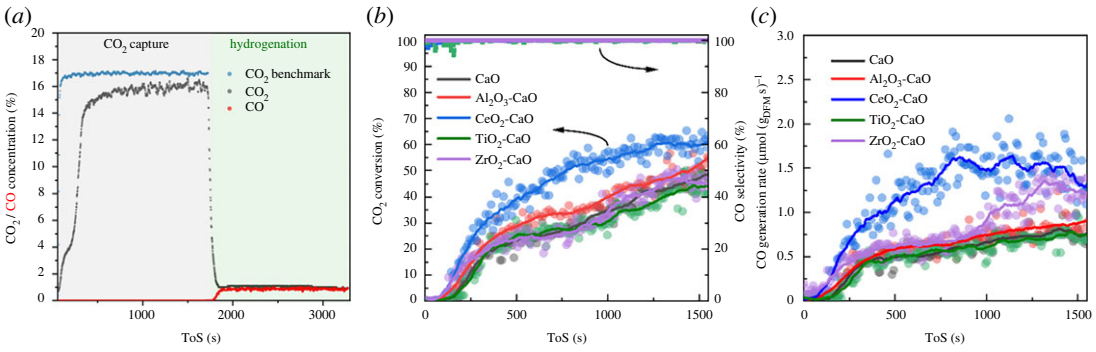

Figure 3. ICCU-RWGS performance of CeO_2-CaO at 650°C (*a*); real-time CO_2 conversion and CO selectivity (*b*) and CO generation rate (*c*) of ICCU-RWGS over MO_x-CaO (M = Al, Ce, Ti or Zr) DFMs at 650°C.

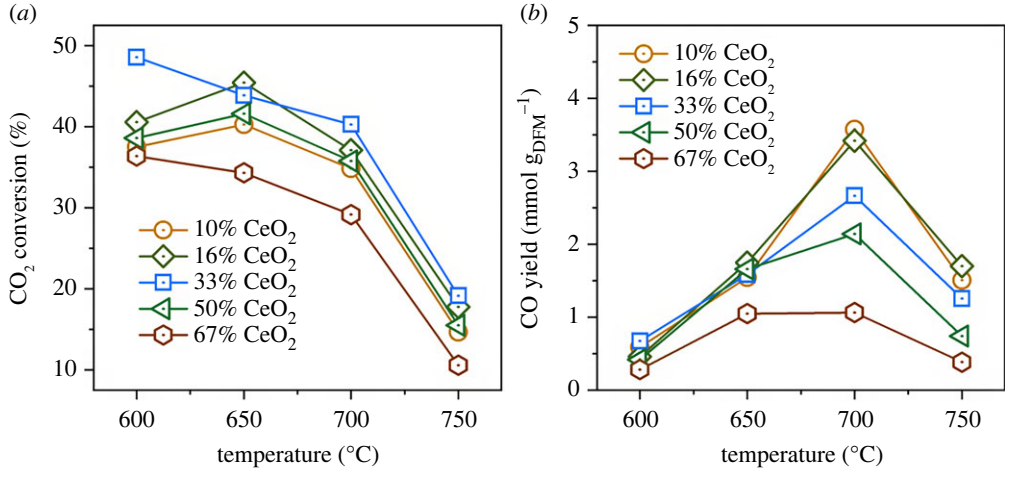

Figure 4. The effect of CeO_2 fraction in CeO_2-CaO DFMs over ICCU-RWGS at various temperature: (*a*) CO_2 conversion and (*b*) CO yield.

The Al_2O_3-CaO and ZrO_2-CaO DFMs, assigned as inert benchmarks, possessed similar ICCU-RWGS performance compared with CaO-alone. In the previous research [26], the CaO-alone was proven active for ICCU-RWGS via direct hydrogenation of carbonates. It can also be concluded that TiO_2 is inactive in ICCU-RWGS according to the poor performance of TiO_2-CaO DFM. And the interaction between TiO_2 and CaO ($CaTiO_3$) performs no promotion effect on CO_2 hydrogenation in ICCU. The CeO_2-CaO outperformed all the other tested DFMs and possessed superior catalytic CO_2 conversion (approx. 60%) and CO generation rate (approx. 1.5 μmol g_{DFM} s^{-1}) at 650°C (figure 3*c*).

3.3 The effect of CeO_2 mass fraction on integrated CO_2 capture and reverse water–gas shift reaction performance

To identify the optimal fraction of CeO_2 in the CeO_2-CaO DFM, a set of DFMs (CeO_2 fraction: 10–67 wt%) were evaluated for ICCU-RWGS performance at a temperature range of 600°C to 750°C (figure 4). The 33 wt% CeO_2 in DFM exhibited the optimal CO_2 conversion at the tested temperatures. The low CeO_2 fraction can restrict the catalytic performance due to the insufficient catalytic sites, while a CeO_2 fraction over 50% can lead to a restriction of the adsorbent amount and hinder the overall CO_2 capture performance of DFM. As can be seen from the CO yield results in figure 4*b*, a lower CeO_2 fraction, representing a higher CaO fraction, could provide more carbonates and thus achieve a higher CO yield. For example, 10% and 67% CeO_2-CaO DFMs achieved 3.5 and 1.0 mmol g_{DFM}^{-1} CO yield at 700°C, respectively.

The reaction temperature is another key parameter in ICCU-RWGS using CeO_2-CaO DFMs. The RWGS is an endothermic reaction [34], which prefers a higher temperature. However, the simultaneous decomposition of $CaCO_3$ is more intense to release excessive CO_2 at higher reaction temperature [35], especially in the tested temperature range. The trade-off between RWGS performance and carbonates decomposition can reflect on

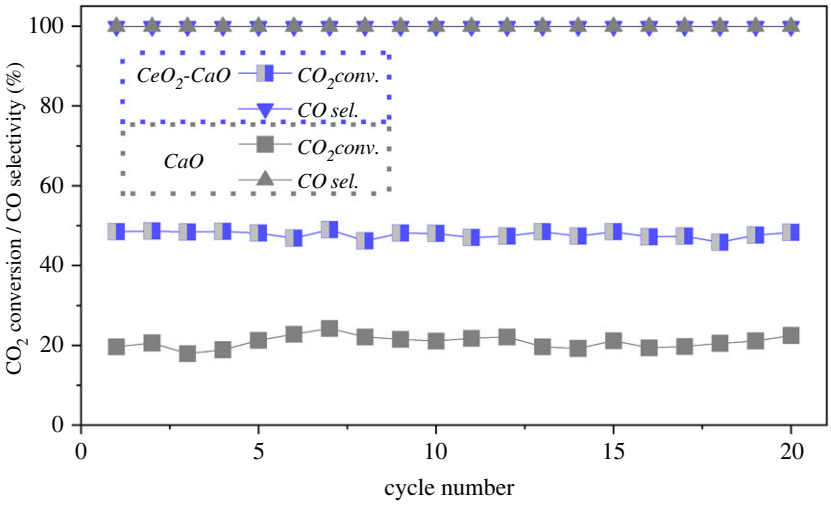

Figure 5. Cycle performance of ICCU-RWGS using 33% CeO_2-CaO DFM at 650°C.

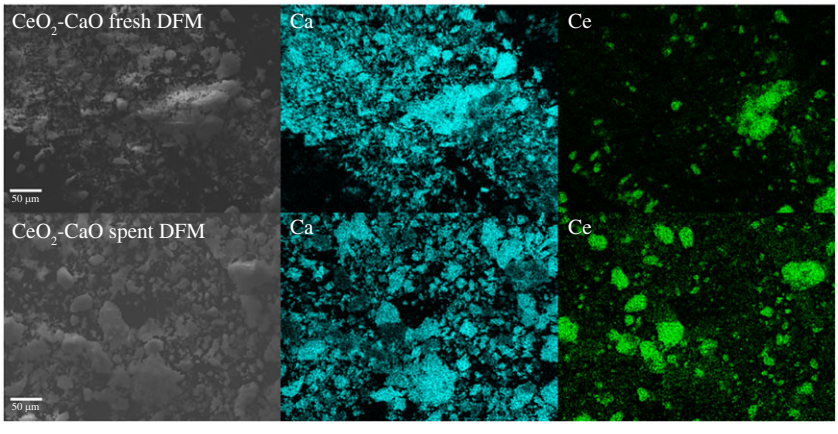

Figure 6. SEM-mapping images of fresh and spent (after 20 cycles) CeO_2-CaO DFM.

CO_2 conversion and CO yield (figure 4). As shown in figure 4*a*, the CeO_2-CaO DFMs possessed relatively higher CO_2 conversion and reasonable CO yield at 650°C in approximately 1700 s hydrogenation, which is proven a suitable temperature for ICCU-RWGS.

3.4. Cycle performance of integrated CO_2 capture and reverse water–gas shift reaction using 33% CeO_2-CaO dual functional material

The cycle stability of the optimal 33% CeO_2-CaO DFM was further evaluated on ICCU-RWGS at the determined suitable reaction temperature of 650°C. As shown in figure 5, 33% CeO_2-CaO possessed impressive stable catalytic performance in 20 reaction cycles. Specifically, the CO_2 conversion and CO selectivity using 33% CeO_2-CaO were sustained at approximately 49% and greater than 99%, respectively. As shown in figure 6, the morphology and chemical composition of CeO_2 and CaO in the catalyst were stable after cyclic evaluation, indicating the outstanding stability of CeO_2-CaO DFM in ICCU-RWGS. Furthermore, the 33% CeO_2-CaO DFM possessed superior catalytic activity (approx. 49%) compared with CaO-alone, which achieved only approximately 20% CO_2 conversion during ICCU-RWGS cycles.

In the previous research, the CeO_2 possessed excellent synergistic catalytic performance due to the oxygen vacancy and abundant coordination defect [18,23,36]. In ICCU-RWGS, the CeO_2 can provide a basic surface (figure 2*c*) to promote CO_2 chemisorption and activation [23]. It is speculated that the CO_2 is decomposed from carbonates, adsorbed on the surface of CeO_2 and activated by its oxygen vacancies [37]. It is also believed that H_2 could interact with ceria to promote CO_2 hydrogenation [38,39]. Notably, the CeO_2-CaO DFM can effectively and selectively (greater than 99%) convert CO_2

into CO in the absence of active metals (e.g. Ni and Ru). It is known that CH_4 formation is highly related to H_2 dissociation [40,41], which hardly occurred in the absence of H_2-sensitive active metals. Although some metals can achieve excellent CO selectivity in ICCU-RWGS via the redox pathway [19], such as Fe, a new drawback arises. Specifically, the Fe will be in the form of a metallic state after hydrogenation, which leads to undesirable CO formation in the following CO_2 capture (equation (3.1)). Compared with that, the CeO_2-CaO DFM demonstrated in this study is evidenced to address the above obstructions on undesirable CO formation but with superior and sustainable catalytic activity to realize a more promising ICCU-RWGS process.

$$M + XCO_2 \rightarrow XCO + MO_X \ (M = \text{Fe, Co etc.}). \tag{3.1}$$

4. Conclusion

ICCU is an emerging process, which provides a more direct path between CO_2-contained exhaust gas and catalytic conversion. The existing DFMs for ICCU-RWGS reaction meet obstructions on low CO selectivity, catalytic efficiency or undesirable CO generation in CO_2 capture. Herein, a non-active metal containing CeO_2-CaO DFM was synthesized to overcome the obstructions using simple and easy-access physically mixing method. The investigation of the effect of different MO_x-CaO (M = Al, Ce, Ti or Zr) DFMs with different mass fraction of MO_x show that CeO_2-CaO DFM with 33 wt% of CeO_2 possessed significantly enhanced and sustainable (20 reaction cycles) ICCU-RWGS catalytic performance. Specifically, approximately 49% CO_2 conversion and approximately 100% CO selectivity were achieved over the 33% CeO_2-CaO DFM. As a comparison, CaO-alone could only realize approximately 20% CO_2 conversion. The superior surface basicity on CeO_2 is believed to contribute to CO_2 chemisorption and activation among all tested MO_x (M = Al, Ce, Ti or Zr). The CeO_2-CaO DFMs exhibit a cost-effective, noble metal-free, stable and highly efficient materials candidates for promising industrial application of ICCU.

Data accessibility. This article has no additional data.

Authors' contributions. S.S.: conceptualization, data curation, investigation, methodology, validation, writing—original draft and writing—review and editing; C.Z.: data curation and investigation; S.C.: data curation and methodology; X.Z.: data curation and investigation; Y.W.: data curation and investigation; S.X.: conceptualization, data curation, funding acquisition, methodology, project administration, resources, supervision, writing—original draft and writing—review and editing; C.W.: conceptualization, data curation, investigation, methodology, project administration, resources, supervision, validation, visualization, writing—original draft and writing—review and editing.

All authors gave final approval for publication and agreed to be held accountable for the work performed therein.

Conflict of interest declaration. We declare we have no competing interests.

Funding. The authors gratefully acknowledge financial support from the China Scholarship Council (reference number: 201906450023). This project has received funding from the European Union's Horizon 2020 research and innovation programme under the Marie Skłodowska-Curie grant agreement no. 823745. The UK Catalysis Hub is kindly thanked for the resources and support provided via our membership of the UK Catalysis Hub Consortium and funded by EPSRC grant: EP/R026939/1, EP/R026815/1, EP/R026645/1, EP/R027129/1 or EP/M013219/1(biocatalysis). The University of Manchester is kindly thanked for funding this research.

References

1. Qin L, Kirikkaleli D, Hou Y, Miao X, Tufail M. 2021 Carbon neutrality target for G7 economies: examining the role of environmental policy, green innovation and composite risk index. *J. Environ. Manage.* **295**, 113119. (doi:10.1016/j.jenvman.2021.113119)
2. Mercure JF *et al.* 2018 Macroeconomic impact of stranded fossil fuel assets. *Nat. Clim. Change* **8**, 588–593. (doi:10.1038/s41558-018-0182-1)
3. Bui M *et al.* 2018 Carbon capture and storage (CCS): the way forward. *Energy Environ. Sci.* **11**, 1062–1176. (doi:10.1039/C7EE02342A)
4. Baena-Moreno FM, Rodríguez-Galán M, Vega F, Alonso-Fariñas B, Vilches Arenas LF, Navarrete B. 2019 Carbon capture and utilization technologies: a literature review and recent advances. *Energy Sources Part A* **41**, 1403–1433. (doi:10.1080/15567036.2018.1548518)
5. Shaw R, Mukherjee S. 2022 The development of carbon capture and storage (CCS) in India: a critical review. *Carbon Capture Sci. Technol.* **2**, 100036. (doi:10.1016/j.ccst.2022.100036)
6. He X, Chen D, Liang Z, Yang F. 2022 Insight and comparison of energy-efficient membrane processes for CO_2 capture from flue gases in power plant and energy-intensive industry. *Carbon Capture Sci. Technol.* **2**, 100020. (doi:10.1016/j.ccst.2021.100020)
7. Hong WY. 2022 A techno-economic review on carbon capture, utilisation and storage systems for achieving a net-zero CO_2 emissions future. *Carbon Capture Sci. Technol.* **3**, 100044. (doi:10.1016/j.ccst.2022.100044)
8. Sun S, Sun H, Williams PT, Wu C. 2021 Recent advances in integrated CO_2 capture and utilization: a review. *Sustain. Energy Fuels* **5**, 4546–4559. (doi:10.1039/D1SE00797A)

9. Merkouri LP, Reina TR, Duyar MS. 2021 Closing the carbon cycle with dual function materials. *Energy Fuels* **35**, 19 859–19 880. (doi:10.1021/acs.energyfuels.1c02729)
10. Shao B, Zhang Y, Sun Z, Li J, Gao Z, Xie Z, Hu J, Liu H. 2021 CO_2 capture and in-situ conversion: recent progresses and perspectives. *Green Chem. Eng.* **3**, 189–198. (doi:10.1016/j.gce.2021.11.009)
11. Qiao Y, Liu W, Guo R, Sun S, Zhang S, Bailey JJ, Fang M, Wu C. 2023 Techno-economic analysis of integrated carbon capture and utilisation compared with carbon capture and utilisation with syngas production. *Fuel* **332**, 125972. (doi:10.1016/j.fuel.2022.125972)
12. Duyar MS, Trevino MAA, Farrauto RJ. 2015 Dual function materials for CO_2 capture and conversion using renewable H_2. *Appl. Catal., B* **168**, 370–376. (doi:10.1016/j.apcatb.2014.12.025)
13. Bermejo-López A, Pereda-Ayo B, Onrubia-Calvo JA, González-Marcos JA, González-Velasco JR. 2022 Tuning basicity of dual function materials widens operation temperature window for efficient CO_2 adsorption and hydrogenation to CH_4. *J. CO_2 Utilization* **58**, 101922. (doi:10.1016/j.jcou.2022.101922)
14. Onrubia-Calvo JA, Bermejo-López A, Pérez-Vázquez S, Pereda-Ayo B, González-Marcos JA, González-Velasco JR. 2022 Applicability of $LaNiO_3$-derived catalysts as dual function materials for CO_2 capture and in-situ conversion to methane. *Fuel* **320**, 123842. (doi:10.1016/j.fuel.2022.123842)
15. Sun S, Sun H, Guan S, Xu S, Wu C. 2022 Integrated CO_2 capture and methanation on Ru/CeO_2-MgO combined materials: morphology effect from CeO_2 support. *Fuel* **317**, 123420. (doi:10.1016/j.fuel.2022.123420)
16. Sun H, Zhang Y, Guan S, Huang J, Wu C. 2020 Direct and highly selective conversion of captured CO_2 into methane through integrated carbon capture and utilization over dual functional materials. *J. CO_2 Utilization* **38**, 262–272. (doi:10.1016/j.jcou.2020.02.001)
17. Shao B *et al.* 2021 Heterojunction-redox catalysts of $Fe_xCo_yMg_{10}CaO$ for high-temperature CO_2 capture and in situ conversion in the context of green manufacturing. *Energy Environ. Sci.* **14**, 2291–2301. (doi:10.1039/D0EE03320K)
18. Sun H, Wang J, Zhao J, Shen B, Shi J, Huang J, Wu C. 2019 Dual functional catalytic materials of Ni over Ce-modified CaO sorbents for integrated CO_2 capture and conversion. *Appl. Catal., B* **244**, 63–75. (doi:10.1016/j.apcatb.2018.11.040)
19. Wang G, Guo Y, Yu J, Liu F, Sun J, Wang X, Wang T, Zhao C. 2022 Ni-CaO dual function materials prepared by different synthetic modes for integrated CO_2 capture and conversion. *Chem. Eng. J.* **428**, 132110. (doi:10.1016/j.cej.2021.132110)
20. Sun S, Zhang C, Guan S, Xu S, Williams PT, Wu C. 2022 Ni/support-CaO bifunctional combined materials for integrated CO_2 capture and reverse water-gas shift reaction: influence of different supports. *Sep. Purif. Technol.* **298**, 121604. (doi:10.1016/j.seppur.2022.121604)
21. Peplow M. 2022 The race to upcycle CO_2 into fuels, concrete and more. *Nature* **603**, 780–783. (doi:10.1038/d41586-022-00807-y)
22. Sun H *et al.* 2021 Understanding the interaction between active sites and sorbents during the integrated carbon capture and utilization process. *Fuel* **286**, 119308. (doi:10.1016/j.fuel.2020.119308)
23. Sun H *et al.* 2022 Integrated carbon capture and utilization: synergistic catalysis between highly dispersed Ni clusters and ceria oxygen vacancies. *Chem. Eng. J.* **437**, 135394. (doi:10.1016/j.cej.2022.135394)
24. Bobadilla LF, Riesco-García JM, Penelás-Pérez G, Urakawa A. 2016 Enabling continuous capture and catalytic conversion of flue gas CO_2 to syngas in one process. *J. CO_2 Utilization* **14**, 106–111. (doi:10.1016/j.jcou.2016.04.003)
25. Sun S, He S, Wu C. 2022 Ni promoted Fe-CaO dual functional materials for calcium chemical dual looping. *Chem. Eng. J.* **441**, 135752. (doi:10.1016/j.cej.2022.135752)
26. Sun S, Lv Z, Qiao Y, Qin C, Xu S, Wu C. 2021 Integrated CO_2 capture and utilization with CaO-alone for high purity syngas production. *Carbon Capture Sci. Technol.* **1**, 100001. (doi:10.1016/j.ccst.2021.100001)
27. Sasayama T, Kosaka F, Liu Y, Yamaguchi T, Chen SY, Mochizuki T, Urakawa A, Kuramoto K. 2022 Integrated CO_2 capture and selective conversion to syngas using transition-metal-free Na/Al_2O_3 dual-function material. *J. CO_2 Utilization* **60**, 102049. (doi:10.1016/j.jcou.2022.102049)
28. Védrine JC. 2019 Metal oxides in heterogeneous oxidation catalysis: state of the art and challenges for a more sustainable world. *ChemSusChem* **12**, 577–588. (doi:10.1002/cssc.201802248)
29. Montini T, Melchionna M, Monai M, Fornasiero P. 2016 Fundamentals and catalytic applications of CeO_2-based materials. *Chem. Rev.* **116**, 5987–6041. (doi:10.1021/acs.chemrev.5b00603)
30. Kosaka F, Liu Y, Chen SY, Mochizuki T, Takagi H, Urakawa A, Kuramoto K. 2021 Enhanced activity of integrated CO_2 capture and reduction to CH_4 under pressurized conditions toward atmospheric CO_2 utilization. *ACS Sustain. Chem. Eng.* **9**, 3452–3463. (doi:10.1021/acssuschemeng.0c07162)
31. Hu J, Hongmanorom P, Galvita VV, Li Z, Kawi S. 2021 Bifunctional Ni-Ca based material for integrated CO_2 capture and conversion via calcium-looping dry reforming. *Appl. Catal., B* **284**, 119734. (doi:10.1016/j.apcatb.2020.119734)
32. Liu P, Niu R, Li W, Wang S, Li J. 2019 Morphology effect of ceria on the ammonia synthesis activity of Ru/CeO_2 catalysts. *Catal. Lett.* **149**, 1007–1016. (doi:10.1007/s10562-019-02674-1)
33. Wang S, Zhao L, Wang W, Zhao Y, Zhang G, Ma X, Gong J. 2013 Morphology control of ceria nanocrystals for catalytic conversion of CO_2 with methanol. *Nanoscale* **5**, 5582–5588. (doi:10.1039/C3NR00831B)
34. Su X, Yang X, Zhao B, Huang Y. 2017 Designing of highly selective and high-temperature endurable RWGS heterogeneous catalysts: recent advances and the future directions. *J. Energy Chem.* **26**, 854–867. (doi:10.1016/j.jechem.2017.07.006)
35. Blamey J, Anthony E, Wang J, Fennell P. 2010 The calcium looping cycle for large-scale CO_2 capture. *Prog. Energy Combust. Sci.* **36**, 260–279. (doi:10.1016/j.pecs.2009.10.001)
36. Dai B, Zhou G, Ge S, Xie H, Jiao Z, Zhang G, Xiong K. 2017 CO_2 reverse water-gas shift reaction on mesoporous M-CeO_2 catalysts. *Can. J. Chem. Eng.* **95**, 634–642. (doi:10.1002/cjce.22730)
37. Dai B, Cao S, Xie H, Zhou G, Chen S. 2018 Reduction of CO_2 to CO via reverse water-gas shift reaction over CeO_2 catalyst. *Korean J. Chem. Eng.* **35**, 421–427. (doi:10.1007/s11814-017-0267-y)
38. Sohlberg K, Pantelides ST, Pennycook SJ. 2001 Interactions of hydrogen with CeO_2. *J. Am. Chem. Soc.* **123**, 6609–6611. (doi:10.1021/ja004008k)
39. Matsuda T, Ishibashi R, Koshizuka Y, Tsuneki H, Sekine Y. 2022 Quantitative investigation of CeO_2 surface proton conduction in H_2 atmosphere. *Chem. Commun.* **58**, 10 789–10 792. (doi:10.1039/D2CC03687H)
40. Shin HH, Lu L, Yang Z, Kiely CJ, McIntosh S. 2016 Cobalt catalysts decorated with platinum atoms supported on barium zirconate provide enhanced activity and selectivity for CO_2 methanation. *ACS Catalysis* **6**, 2811–2818. (doi:10.1021/acscatal.6b00005)
41. Ashok J, Pati S, Hongmanorom P, Tianxi Z, Junmei C, Kawi S. 2020 A review of recent catalyst advances in CO_2 methanation processes. *Catal. Today* **356**, 471–489. (doi:10.1016/j.cattod.2020.07.023)